

Improved Lemaitre-Tolman model and the mass and turn-around radius in group of galaxies

Antonino Del Popolo^{a,b}, Maksym Deliyergiyev^{c,2}, and Man Ho Chan^d

^aDipartimento di Fisica e Astronomia, University Of Catania, Viale Andrea Doria 6, 95125, Catania, Italy; ^bInstitute of Astronomy, Russian Academy of Sciences, Pyatnitskaya str. 48, 119017 Moscow, Russia; ^cDépartement de Physique Nucléaire et Corpusculaire, University of Geneva, CH-1211 Geneve 4, Switzerland; ^dDepartment of Science and Environmental Studies, The Education University of Hong Kong, Tai Po, New Territories, Hong Kong

We extended the modified Lemaitre-Tolman model Ref.(1, 2) taking into account the effect of angular momentum and dynamical friction. The inclusion of these quantities in the equation of motion modifies the evolution of a perturbation, initially moving with the Hubble flow. Solving the equation of motions we got the relationships between mass, M , and the turn-around radius, R_0 . Knowing R_0 , the quoted relation allows the determination of the mass of the object studied. The relationships for the case in which also the angular momentum is taken into account gives a mass $\simeq 90\%$ larger than the standard Lemaitre-Tolman model, and two times the value of the standard Lemaitre-Tolman model, in the case also dynamical friction is taken into account. As a second step, we found relationships between the velocity, v , and radius, R , and fitted them to data of the Local Group, M81, NGC 253, IC342, CenA/M83, and to the Virgo clusters obtained by Ref.(1, 2). This allowed us to find optimized values of the mass and Hubble constant of the objects studied. The fit gives values of the masses smaller with respect to the $M - R_0$ relationship method, but in any case 30-40% larger than the $v - R$ relationship obtained from the standard Lemaitre-Tolman model. Differently from mass, the Hubble parameter becomes smaller with respect to the standard Lemaitre-Tolman model, when angular momentum, and dynamical friction are introduced. This is in agreement with Ref.(1, 2), who improved the standard Lemaitre-Tolman model taking into account the cosmological constant.

Finally, we used the mass, M , and R_0 of the studied objects to put constraints to the dark energy equation of state parameter, w . Comparison with previous studies show different constraints on w .

dwarf galaxies | galaxy clusters | modified gravity | mass-temperature relation

While the mass-to-light (M/L) ratios of group of galaxies was in the past estimated through the virial theorem to be typically of the order of $\simeq 170M_\odot/L_{B,M_\odot}$ Ref.(3), new measurements based on high quality data, and estimating methods different from the Virial theorem Ref.(4) give much smaller results in the range $10 - 30M_\odot/L_{B,M_\odot}$. This means that the local matter density should be a fraction of the global one. It is well known that the virial theorem gives reliable results if the system is in dynamical equilibrium. This condition is often assumed if the crossing time is less than the Hubble time. This assumption has been shown to be often not correct by Ref.(5), whose analysis showed that there is no correlation between the virial ratio $\frac{2T}{W}$, being T , and W the kinetic and potential energy, and the crossing time. By means of methods used by observers, Ref.(5) showed that $\simeq 20\%$ of the studied groups were not gravitationally bound. Ref.(6) and Ref.(7) proposed an alternative approach to the virial theorem based on the Lemaitre-Tolman (LT) model Ref.(8, 9) giving a good description of a central core gravitationally bound located inside an homogeneous region whose density decreases till reach-

ing the background value. The model describes the evolution of the system in a similar way to that done by the spherical collapse model. Considering a shell of given radius containing a mass M , it initially expands following the Hubble flow. When the density overcomes a critical value the shell reaches a maximum radius, known as turn-around radius, R_0 , characterized by zero velocity, and collapses. Then in the LT model there is a central region in equilibrium, surrounded by a region which reaches its maximum expansion and collapses, and a zero totally energy region constituted by shells still bound to the structure and unbound ones. Because of its characteristics, the LT model gives a good description of a group of galaxies dominated by one or two central galaxies embedded into a cloud of smaller ones. If using the velocity field around the main bodies allows the determination of the turn-around radius R_0 , the mass can be obtained through the relation

$$M = \frac{\pi^2 R_0^3}{8GT_0^2} \quad [1]$$

Refs.(1, 2, 7), where T_0 is the age of the universe. The quoted model was applied to the local group Ref.(7) and to the Virgo cluster Refs.(10–12). The model was modified taking into account the cosmological constant by Ref.(1, 2) applying it to the Virgo cluster, the pair M31-MW, M81, the Centaurus A-M83 group, the IC342/Maffei-I group, and the NGC 253 group. As shown in Refs.(1, 2) the introduction of the cosmological constant modifies the mass, M , turn-around radius, R_0 , relation. As a consequence for a given R_0 , the value of the mass of the system is $\simeq 30\%$ larger with respect to Eq. (1) Refs.(1, 2), while the Hubble constant of the modified model is smaller than the standard LT.

In order to obtain the mass of the previously quoted objects, Refs.(1, 2), differently from Ref.(7), did not use the standard LT (SLT) $M - R_0$ relation (Eq. (1)). They built up a velocity-distance relationship, $v - R$, describing the kinematic status of the systems studied. Knowing the values of v , and r for the members of the groups studied, the mass of the group, M , and the Hubble parameter can be obtained by means of a non-linear fit of the $v - R$ relation to the data.

In the present paper, we will further extend the modified Lemaitre-Tolman (MLT model) by taking into account the effect of angular momentum (JLT model) and dynamical friction (J η LT model). The effect of these two quantities on the spherical collapse model (SCM) and its effect on the clusters of galaxies structure and evolution, the turn-around, the threshold of collapse, their mass function, their mass-temperature relation, have been studied in Refs.(13–21).

² E-mail: maksym.deliyergiyev@unige.ch

Similarly to Ref.(1, 2), we will find the $v - R$ relation by solving the equation of the SCM, and then fit it to the data of the Virgo cluster, the pair M31-MW, M81, the Centaurus A-M83 group, the IC342/Maffei-I group, and the NGC 253 group.

The paper is organized as follows. In Section , we introduce the model, and solve it. In Section , we find the velocity-radius relation for the JLT, and $J\eta$ LT models. In Section , we applied the $v - R$ relation to groups and clusters of galaxies. In Section , we studied the impact of the angular momentum and dynamical friction on the $M - R_0$ relation. In Section , we showed how the obtained values of M and R_0 may constrain the dark energy equation of state parameter, w . Section is devoted to conclusions.

Model

The simplest form of the SCM was introduced by Ref.(22). It is a simple and popular method to study analytically the non-linear evolution of perturbations of dark matter (DM) and dark energy (DE). As previously reported, the model describes the evolution of a spherical symmetric over density which initially expands with the Hubble flow, then detaches from it, when the density overcomes a critical value, reaches a maximum radius, dubbed turn-around radius, and finally collapse and virialize. SCM is a very simple model assuming that matter moves in a radial fashion Ref.(22–24). Tidal angular momentum Ref.(25, 26), random angular momentum Refs.(27–29), dynamical friction (Refs.(30, 31)), etc., are not taken into account. Later the SCM was improved in several papers Ref.(27, 29, 32–36), adding the cosmological constant Ref.(37), and tidal and random angular momentum(27, 29, 36, 38–45)*. Dynamical friction was studied in Refs.(30, 31), while Refs.(46–48) discussed the role of shear in the gravitational collapse.

The SCM with negligible DE perturbations was extensively investigated in literature Refs.(see, e.g. 49–55), while DE fluid perturbation were taken into account in Refs.(see 56–64). Using the non-linear differential equations for the evolution of the matter density contrast derived from Newtonian hydrodynamics in Ref.(54), Ref.(65) showed that the parameters of the SCM become mass dependent.

Refs.(65, 66) studied the effects of shear and rotation in smooth DE models. The effects of shear and rotation were investigated in Refs.(65, 66) for smooth DE models, Ref.(67) in clustering DE cosmologies, and Ref.(68) in Chaplygin cosmologies.

In this paper, we are interested in describing a system constituted by a dominant mass concentration, and satellites that are not contributing significantly to the group mass, and that further mass accretion is neglected.

The equation of motion of the system may be obtained as follows. We consider some gravitationally growing mass concentration collecting into a potential well. Let us assume that the probability of a particle, located at $[r, r + dr]$, having angular momentum $L = rv_\theta$, defined in the range $[L, L + dL]$, with velocity $v_r = \dot{r}$, defined in the range $[v_r, v_r + dv_r]$, has the following form

$$dP = f(L, r, v_r, t)dLdv_rdr. \quad [2]$$

* Particles angular momenta is randomly distributed in random such that the mean angular momentum at any point in space is zero Ref.(40, 42) then conserving spherical symmetry and angular momentum.

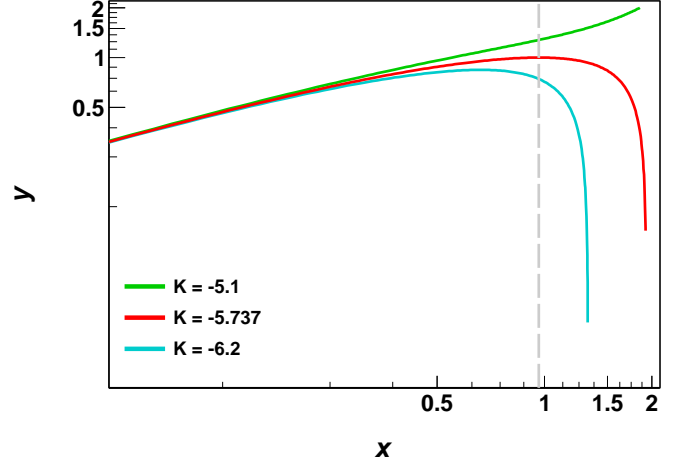


Fig. 1. Evolution of shell radius for different values of K . The red, cyan, and green lines correspond to $K = -5.737$, $K = -6.2$, and $K = -5.1$, respectively.

The term L takes into account ordered angular momentum generated by tidal torques and random angular momentum (see Appendix C.2 of Ref.(31)). The radial acceleration of the particle Refs.(13, 14, 37, 69, 70) is:

$$\frac{dv_R}{dt} = -\frac{GM}{R^2} + \frac{L^2(R)}{M^2R^3} + \frac{\Lambda}{3}R - \eta\frac{dR}{dt}, \quad [3]$$

with Λ being the cosmological constant and η the dynamical friction coefficient. The previous equation can be obtained via Liouville's theorem Ref.(14). The last term, the dynamical friction force per unit mass, η , is explicitly given in Ref.(31) (Appendix D, Eq. D5). A similar equation (excluding the dynamical friction term) was obtained by several authors Refs.(e.g., 65, 71, 72)) and generalized to smooth DE models in Ref.(73).

In terms of the specific angular momentum $J = \frac{L}{M}$, and $\Omega_\Lambda = \frac{\rho_\Lambda}{\rho_c}$, where ρ_c is the critical density, Eq. (3) can be written as

$$\frac{dv_R}{dt} = -\frac{GM}{R^2} + \frac{J^2}{R^3} - \frac{1+3w}{2}\Omega_\Lambda H_0^2 \left(\frac{a_0}{a}\right)^{3(1+w)} R - \eta\frac{dR}{dt}, \quad [4]$$

where w is the DE equation of state (EoS) parameter. DE is modeled by a fluid with an EoS $P = w\rho$, where ρ is the energy density. a is the expansion parameter. Eq. (4) satisfies equation

$$H = \frac{\dot{a}}{a} = H_0 \sqrt{\Omega_m \left(\frac{a_0}{a}\right)^3 + \Omega_\Lambda \left(\frac{a_0}{a}\right)^{3(1+w)}}. \quad [5]$$

In the following, we will treat the case $w = -1$, in other words we assume that DE is the cosmological constant. With this assumption, and assuming that $J = kR^\alpha$, with $\alpha = 1$, in agreement with Ref.(74)[†], and k constant. In terms of the variables $y = R/R_0$, $t = x/H_0$, Eq. (4), and Eq. (5) can be written as

$$\frac{d^2y}{dx^2} = -\frac{A}{2y^2} + \Omega_\Lambda y + \frac{K_j}{y} - \frac{\eta}{H_0} \frac{dy}{dx}, \quad [6]$$

[†] In that paper $\alpha = 1.1 \pm 0.3$

model	η/H_0	K_J	b	n	A
MLT	–	0.0	1.4054	0.6293	3.6575
JLT	–	0.78	1.3759	0.7549	5.0370
J η LT	0.5	0.78	1.3436	0.9107	6.0500

Table 1. The constant A , and the fitting parameters b , and n of the velocity-distance ($v - R$) relations, for the MLT, the JLT, and the J η LT model.

where $K_j = k \frac{1}{(H_0 R_0)^2}$, $A = \frac{2GM}{H_0^2 R_0^3}$, and

$$H = H_0 \sqrt{\Omega_m \left(\frac{a_0}{a}\right)^3 + \Omega_\Lambda}. \quad [7]$$

Eq. (6) has a first integral, given by

$$\begin{aligned} u^2 &= \left(\frac{dy}{dx}\right)^2 \\ &= \frac{A}{y} + \Omega_\Lambda y^2 + 2K_j \log y - 2\frac{\eta}{H_0} \int \left(\frac{dy}{dx}\right)^2 dx + K \end{aligned} \quad [8]$$

where $K = \frac{2E}{(H_0 R_0)^2}$, and E is the energy per unit mass of a shell.

Eqs.(5), and (6) were solved as described in Ref.(1, 2). There are a couple of ways of doing that. A first way, is to obtain the value of the scale parameter and the corresponding time for a given redshift. At high redshift, the gravitational term dominates and through a Taylor expansion one can get the initial conditions. In order to get the parameter A , it is varied until the condition $\frac{dy}{dx} = 0$, and $y = 1$ are satisfied. A second way to get A , is to use the equation for the velocity (Eq. (8)).

Let's show this second method in the case cosmological constant, and angular momentum are present (JLT case)

$$\frac{d^2 y}{dx^2} = -\frac{A}{2y^2} + \Omega_\Lambda y + \frac{K_j}{y} \quad [9]$$

having the first integral

$$u^2 = \left(\frac{dy}{dx}\right)^2 = \frac{A}{y} + \Omega_\Lambda y^2 + 2K_j \log y + K \quad [10]$$

At the turn-around point Eq. (10) gives: $K = -A - \Omega_\Lambda$.

At high redshifts ($z = 1000$), or $y \ll 1$, as was described the gravitational term dominates, and by a Taylor expansion one gets the relation $y \simeq \left(\frac{9A}{4}\right)^{1/3} x^{2/3}$. Assuming an initial value of y , $y_i = 0.001$, corresponding approximately to 1 kpc, the initial time x_i can be obtained. The initial value of the velocity u_i can be obtained, when A is known, through Eq. (10), recalling that $y_i = 0.001$. The value of A is obtained as follows. Eq. (10) can be written as

$$x = \int_{y_i}^1 \frac{dy}{\sqrt{\frac{A}{y} + \Omega_\Lambda y^2 + \frac{K_j}{y} - A - \Omega_\Lambda}} \quad [11]$$

Eq. (7), recalling that $\frac{a_0}{a} = 1 + z$, can be written as

$$x(y = 1) = \int_0^\infty \frac{dz}{(1+z)\sqrt{\Omega_\Lambda + \Omega_m(1+z)^3}} = 0.964. \quad [12]$$

For $\Omega_\Lambda = 0.7$, $\Omega_m = 0.3$, $K_j = 0.78^\ddagger$, $x = 0.964$, Eq. (11) can be solved to get $A = 5.037$. In the case, $K_j = 0$, $A = 3.6575$, and if $K_j = 0$, $\Omega_\Lambda = 0$, the SLT gives $A = 2.655$.

In the case J η LT (Eqs.(6)-(8)), A can be obtained similarly to the previous case (JLT) solving numerically Eq. (8) with the initial condition on y_i , and varying A until the condition $\frac{dy}{dx} = 0$, and $y = 1$ are satisfied. Similarly, we can solve Eq. (6) with the initial condition y_i , and varying A until the condition $\frac{dy}{dx} = 0$, and $y = 1$ are satisfied. In this way, one gets $A = 6.05$.

Now, we show the solution for the case JLT. Eq. (9) can be solved with the conditions $y_i = 0.001$, and

$$\begin{aligned} u(0) &= \sqrt{\frac{5.037}{y_i} + 0.7y_i^2 + 2K_j \log y_i - 0.7 - 5.037} \\ &= 70.833943. \end{aligned} \quad [13]$$

In Fig.1, we plot the result of the solution. The red line corresponds to the case $K = -A - \Omega_\Lambda = -5.737$, being $A = 5.037$. This solution is the one that has just reached the maximum expansion, or turn-around, and the collapse happens in $\simeq 13.8$ Gyr. The cyan line is characterized by $K = -6.2$. It reached the turn-around in the past. Turn-around will happen only for $K < -5.56812$, for larger values the collapse will never occur, as the case of the green line characterized by $K = -5.1$.

The velocity-radius relation

In order to get the mass, and turn-around radius of some groups of galaxies, we will find a relation between the velocity, and radius, $v - R$, that will be fitted to the data. The $v - R$ relation is obtained as follows. Let's consider Fig.1. The vertical line corresponds to $x = 0.964$. Its intersection with the curves, solution of the equations described in the previous section, gives the value $y(x) = y(0.964)$. The solution of the equations of the previous section, also gives the velocity, allowing us to find $u(x) = u(0.964)$. We will get a couple of value (y, u) for each intersection of the vertical line with the curves (see Fig.2 caption for an extended description). This allows us to find a series of points that can be fitted with a relation of the form $u = -b/y^n + by$. For example in the case of the MLT, we get

$$v = -\frac{1.4054}{y^n} + 1.4054y \quad [14]$$

where $n = 0.6293$. This can be written in terms of the physical units as

$$v(R) = -bH_0 R_0 \left(\frac{R_0}{R}\right)^n + bH_0 R \quad [15]$$

where $b = 1.4054$. Substituting in this equation, $R_0 = \left(\frac{2GM}{H_0^2}\right)^{1/3}$, we get

$$v(R) = -b\frac{H_0}{R^n} \left(\frac{2GM}{AH_0^2}\right)^{\frac{n+1}{3}} + bH_0 R \quad [16]$$

or

$$v(R) = -\frac{-1.013H_0}{R^n} \left(\frac{GM}{H_0^2}\right)^{\frac{n+1}{3}} + 1.4054H_0 R \quad [17]$$

[‡]The value of K_j was obtained recalling that term related to angular momentum, L , in Eq. (4), is given by $\frac{L^2}{M^2 R^3}$.

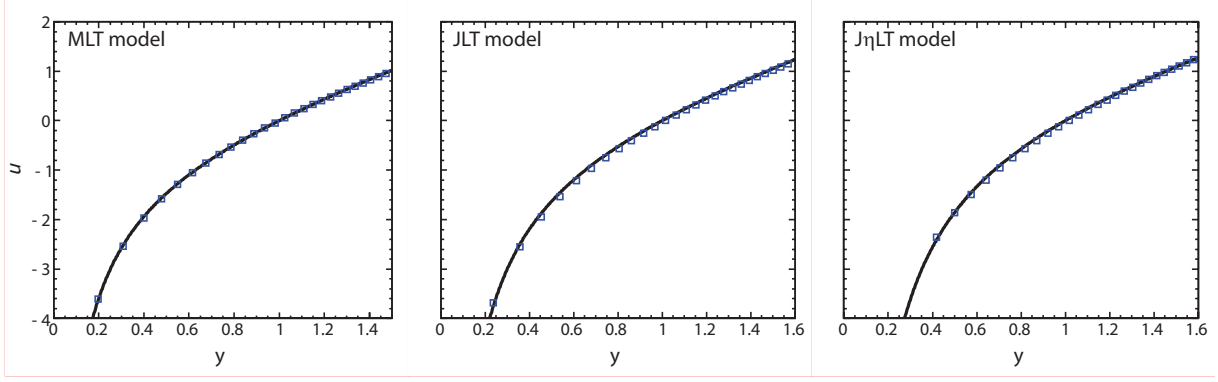


Fig. 2. The velocity profile in the three cases studied. The left panel shows the MLT model. The central panel, the JLT. The right panel, the $J\eta$ LT case. Data points are obtained as follows. Fig. 1, shows some solutions of Eq. 6 for different values of K : $K = -6.2, -5.737, \text{ and } -5.1$. We obtained several solution relative to different values of K : K_1, K_2, K_3, \dots . The intersection of each solution with the vertical axis $x = 0.964$, gives a corresponding value of $y: y_1, y_2, y_3, \dots$. The solution of Eq. 6 for different values of K at $x = 0.964$ gives also u_1, u_2, u_3, \dots . All this gives us a pair of values (y_i, u_i) for each intersection of the vertical line with the curves. The solid black lines are the fit to the points in the examined models.

This relation is slightly different from that obtained by Ref.(2), probably due to the noteworthy sensitivity of the solution of the equation to initial conditions, and to the fact we used more digits in the initial condition for $u(0)$ §.

For this reason, in the rest of the paper, we also consider the MLT case, already studied by Ref.(2). In a similar way, we can obtain the $v - R$ relation in the case the of the JLT model

$$v(R) = -\frac{-0.80155H_0}{R^n} \left(\frac{GM}{H_0^2} \right)^{\frac{n+1}{3}} + 1.3759H_0R \quad [18]$$

where $n = 0.7549$, and in the complete case (cosmological constant, angular momentum, and dynamical friction)

$$v(R) = -\frac{-0.66385H_0}{R^n} \left(\frac{GM}{H_0^2} \right)^{\frac{n+1}{3}} + 1.3436H_0R \quad [19]$$

where $n = 0.9107$. In Fig.2 we plot, from left to right, the velocity profile of the MLT, JLT, and $J\eta$ LT cases, using adimensional variables.

All the previous equations satisfy the condition $v(R_0) = 0$. In the following, we will apply Eq. (19), related to the $J\eta$ LT model to some groups of galaxies and clusters. In Table 1, we summarize the parameters of the different models that were described in this paper. The first line corresponds to the MLT model. The second line to the JLT model, and, the last line to the $J\eta$ LT case,

Table 1, as well as Fig.2 shows that including the angular momentum, and dynamical friction steepens the velocity profile, and increases the parameter A . This means that for a given R_0 the mass of the structure increases, while the radius of the zero-gravity surface decreases.

Application to near groups and clusters of galaxies

Now, we will apply Eqs.(17-19) to near groups and a cluster of galaxies. To this aim, we need for each galaxy its velocity and distance with respect to center of mass. We will use data obtained by Refs.(1, 2). Velocities were transformed from the

heliocentric to the Local Group rest frame. The distance can be written as

$$R = \sqrt{D^2 + D_g^2 - 2DD_g \cos \theta} \quad [20]$$

where the angle θ is the angle between the center of mass and the galaxy, D the distance from the galaxy to the center of mass, and D_g is the distance to the galaxy. Indicating with V , and V_g the center of mass velocities, and that of the galaxy with respect the Local Group rest frame, the velocity difference along the radial direction between both object is

$$V(R) = V_g \cos \alpha - V \cos \beta \quad [21]$$

being $\alpha = \frac{D \sin \theta}{D_g - D \cos \theta}$, and $\beta = \alpha + \theta$.

Since in the list given by Ref.(2) unbound objects, and uncertain distances and velocities were excluded, an error of 10% was considered for velocities and distances by Ref.(2). This value of uncertainty is a weighted mean of data including measurement errors and data reported without errors Ref.(76, 81).

In the case of the group M31-MW, the data were obtained by Ref.(1) from Ref.(75) data. We used the data of Ref.(1) also for the case of the Virgo cluster.

Fig.3 plots the $v - R$ relationships for the groups studied: the M31-MW group (top left panel), the M81 group (top right panel), the NGC 253 group (central left panel), the IC 342 group (central right panel), the CenA/M83 group (bottom left panel), the Virgo cluster (bottom right panel). The red squared are the data from Refs.(1, 2).

M31-MW. We applied Eqs. (17-18), and Eq. (19) to the Ref.(1) data. Both the mass and the Hubble parameter were allowed to vary. The results are shown in Table 2. Ref.(75) estimated a turn-around radius of 0.94 ± 0.1 Mpc and using the SLT model obtained a mass of $1.5 \times 10^{12} M_\odot$, which is much smaller than the estimate of Ref.(1) $(2.5 \pm 0.7) \times 10^{12} M_\odot$, $R_0 = 1.0 \pm 0.1$ Mpc, and $h = 0.74 \pm 0.04$. The value of the mass is larger than that of Ref.(75), that used the SLT model. A tendency of the LT models is that of giving higher masses, and smaller h if the effect of the cosmological constant, angular momentum, and other effects which contribute with positive terms in the equation of motion are taken into account. In fact, Ref.(1)

§This was confirmed via a private discussion with one of the authors of Ref.(2), namely de Freitas Pacheco.

Table 2. Characteristic parameters of the examined groups. The rows 1-3 represent the value of the Hubble parameters for the MLT, JLT, and $J\eta$ LT models. The rows 4-6 the masses of the groups in units of $10^{12}M_{\odot}$ for the same cases, and the rows -9 the values of the turn-around radius, R_0 , in Mpc, for the same cases. The last three rows give the velocity dispersion resulting from the fit of data to the $v - R$ relation for the same cases.

	M31/MW	M81	NGC 253	IC 342	CenA/M83	Virgo
$h(\Omega_{\Lambda} = 0.7)$	0.73 ± 0.04	0.68 ± 0.04	0.63 ± 0.06	0.58 ± 0.10	0.57 ± 0.04	0.71 ± 0.08
$h(j)$	0.70 ± 0.04	0.65 ± 0.04	0.63 ± 0.06	0.56 ± 0.10	0.55 ± 0.04	0.65 ± 0.09
$h(j, \eta)$	0.69 ± 0.04	0.65 ± 0.04	0.63 ± 0.05	0.55 ± 0.10	0.55 ± 0.04	0.59 ± 0.09
$M(\Omega_{\Lambda} = 0.7) [10^{12}M_{\odot}]$	2.49 ± 0.50	1.14 ± 0.10	0.14 ± 0.15	0.22 ± 0.12	2.16 ± 0.50	1493 ± 200
$M(j) [10^{12}M_{\odot}]$	3.090 ± 0.50	1.320 ± 0.10	0.195 ± 0.10	0.263 ± 0.10	2.655 ± 0.50	1585 ± 200
$M(j, \eta) [10^{12}M_{\odot}]$	3.570 ± 0.40	1.398 ± 0.10	0.244 ± 0.10	0.292 ± 0.10	3.015 ± 0.40	1525.55 ± 200
$R_0(\Omega_{\Lambda} = 0.7) [\text{Mpc}]$	1.038 ± 0.10	0.840 ± 0.05	0.440 ± 0.10	0.540 ± 0.09	1.160 ± 0.08	8.850 ± 0.80
$R_0(j) [\text{Mpc}]$	1.04 ± 0.10	0.81 ± 0.05	0.44 ± 0.10	0.53 ± 0.09	1.14 ± 0.08	8.67 ± 0.80
$R_0(j, \eta) [\text{Mpc}]$	1.02 ± 0.10	0.78 ± 0.05	0.44 ± 0.10	0.52 ± 0.09	1.13 ± 0.08	8.56 ± 0.80
$\sigma(\Omega_{\Lambda} = 0.7) [\text{km/s}]$	37.3	51.16	45.58	33.49	44.72	352.1
$\sigma(j) [\text{km/s}]$	38.3	53.24	45.8	33.93	44.75	352.88
$\sigma(j, \eta) [\text{km/s}]$	38.8	54.77	45.9	34.48	44.81	355.1

found a values of $h = 0.87 \pm 0.05$ when using the SLT model, and $h = 0.73 \pm 0.04$ in the MLT case.

The values of R_0 , in all three cases (MLT, JLT, and $J\eta$ LT) are in agreement, within the estimated uncertainties, with estimate reported in Ref.(1). Our values of h , and M are in agreement to that of Ref.(1) in the MLT, JLT, cases, while in the $J\eta$ LT the value is slightly larger. The average value of h is smaller in the JLT, and $J\eta$ LT models, while the reverse happens to the mass. We recall that the errors, come from the fitting procedure.

The M81 group. The M81 group was studied by Refs.(75–77). The authors found $R_0 = 0.89 \pm 0.05$ Mpc, smaller than our estimates, and $M = (1.03 \pm 0.17) \times 10^{12}M_{\odot}$, in agreement only with our MLT case. Ref.(2) found $M = (0.92 \pm 0.24) \times 10^{12}M_{\odot}$, smaller than our cases JLT, and $J\eta$ LT and $h = 0.67 \pm 0.04$, in agreement with all our cases. Our JLT, and $J\eta$ LT model estimates, as in the previous, and in all cases, gives average values of the mass, M larger than the average of the estimates of Refs.(2, 77).

The NGC253 group. Concerning this group, Ref.(78) obtained $R_0 = 0.7 \pm 0.1$ Mpc, smaller than our estimates, and $M = (5.5 \pm 2.2) \times 10^{11}M_{\odot}$, larger than our estimates. Ref.(2) found $M = (1.3 \pm 1.8) \times 10^{11}M_{\odot}$ whose larger uncertainties is probably due to incompleteness in the data. They also found $h = 0.63 \pm 0.06$. Both their estimates for h , and M , are in agreement with all our cases.

The IC342 group. According to Ref.(79), the group has $R_0 = 0.9 \pm 0.1$, and $M = (1.07 \pm 0.33) \times 10^{12}M_{\odot}$, both larger than our estimates. Ref.(2) found a smaller value of the mass, $M = (2.0 \pm 1.3) \times 10^{11}M_{\odot}$, and also $R_0 (\simeq 0.53$ Mpc), while $h = 0.57 \pm 0.10$. Our values of mass, turn-around radius, and h agree with Ref.(2) estimates.

The CenA/M83 group. This group was studied by Refs.(80, 81). From the distances, and velocities of the group member, taking into account the cosmological constant they found $R_0 = 1.55 \pm 0.13$ Mpc, and $M = (6.4 \pm 1.8) \times 10^{12}M_{\odot}$, larger than our estimates. Ref.(82), using different mass indicators found a larger mass ($M = (9.2 \pm 3) \times 10^{12}M_{\odot}$). Ref.(2), found values 3-4 times smaller ($M = (2.1 \pm 0.5) \times 10^{12}M_{\odot}$),

and $h = 0.57 \pm 0.04$. In our analysis, both M , and h are in agreement with Ref.(2).

The Virgo cluster. Concerning Virgo, several estimates for the mass were done by means of the SLT model Ref.(10, 83), by means of the Virial theorem Ref.(11) finding masses smaller than $10^{15}M_{\odot}$, except Ref.(83) who found a value of $1.3 \times 10^{15}M_{\odot}$. Using the MLT model Ref.(1) found $M = (1.10 \pm 0.12) \times 10^{15}M_{\odot}$, $h = 0.65 \pm 0.09$, and $R_0 = 8.6 \pm 0.8$ Mpc. Our estimates are in agreement with the value of h , R_0 of Ref.(1), while the masses in the cases JLT, and $J\eta$ LT are larger than in Ref.(1).

In summary, our estimates usually agree with the estimates of Ref.(1, 2), especially in the case MLT, and JLT. In some cases there are discrepancies with the predictions of our $J\eta$ LT model. Moving from the SLT model to the MLT, JLT, and $J\eta$ LT, the values of the cosmological constant decreases, and the opposite happens to the mass, M .

Another important issue that is shown by Table 2, is that the values of h are in some cases smaller than the known estimates. In the past decade or so, has been performed dozens of measurements of the Hubble constant, to try to overcome the Hubble constant tension. As clear shown from Ref.(84), from the year 2000 the constraints have changed from 72_{-8}^{+8} km/Mpc s, to the range 67–75 km/Mpc s. Recent constraints from the gravitational wave signal of GW170817 gives $70.3_{-5.0}^{+5.3}$ km/Mpc s Ref.(85), $67.4_{-1.2}^{+1.1}$ km/Mpc s (DES + BAO + BBN), and 67.5 ± 1.1 km/Mpc s Ref.(86). The previous constraints are in agreement with our results, except for CenA/M83 having $H = 59$ km/Mpc s. The last discrepancy with observations may be due to non completeness of the data used in 2008 by Ref.(2). Based on a large-scale survey of the Centaurus group done in 2014-2015, a significant amount of faint dwarf galaxy candidates were discovered Ref.(87). Therefore, the old data used in Ref.(2) may contain some selection bias so that the resulting H obtained is systematically smaller.

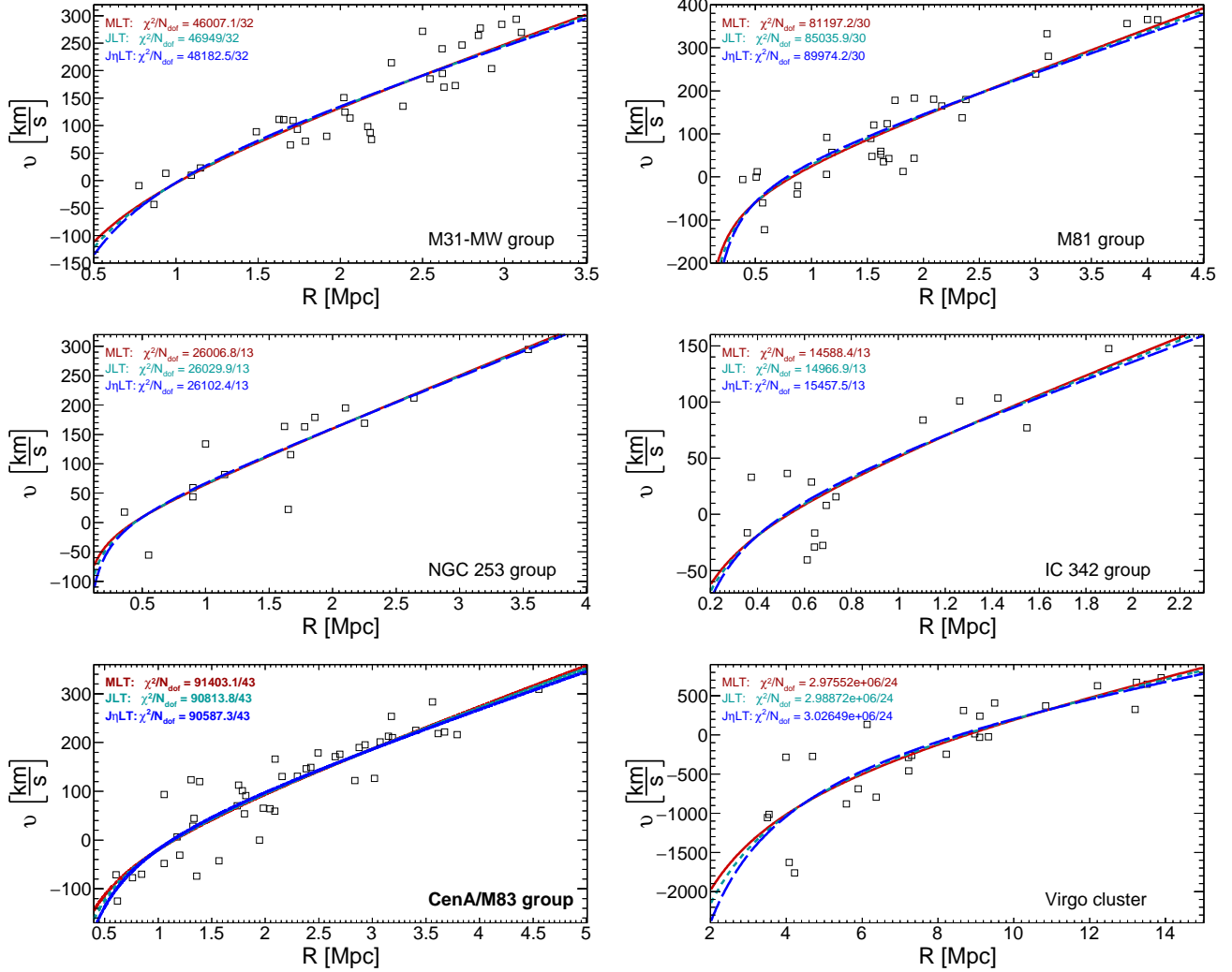


Fig. 3. Velocity-distance plots for the M31-MW group (top left panel), the M81 group (top right panel), the NGC 253 group (central left panel), the IC 342 group (central right panel), the CenA/M83 group (bottom left panel), the Virgo cluster (bottom right panel). The black dots are the data from Ref.(1, 2). Red solid lines correspond to the fit with the MLT model, Eq. (17), cyan short dashed lines – JLT model, Eq. (18), blue dashed lines – $J\eta$ LT model, Eq. (19). The χ^2/N_{dof} values were added into each panel only in illustrative purpose, since the exact uncertainties of the data unknown.

Effects of cosmological constant, angular momentum, and dynamical friction

As we wrote in the Introduction, the mass predicted by the LT model is given by Eq. (1), namely

$$M = \frac{\pi^2 R_0^3}{8GT_0^2} = 3.06 \times 10^{12} h^2 R_0^3 M_\odot \quad [22]$$

For the MLT, the value of A can be obtained combining Eq. (11), and Eq. (12), and one gets $A = 3.6575$. By the definition of $A = \frac{2GM}{H_0^2 R_0^3}$, and recalling that in the Λ CDM model $H_0 = f(\Omega)/T_0$, where

$$f(\Omega) = \int_0^\infty \frac{dz}{(1+z)\sqrt{\Omega_\Lambda + \Omega_m(1+z)^3}} \quad [23]$$

we obtain, for $\Omega_\Lambda = 0.7$

$$M = \frac{1.82875 H_0^2 R_0^3}{G} = \frac{1.69945 R_0^3}{GT_0^2} = 4.22 \times 10^{12} h^2 R_0^3 M_\odot \quad [24]$$

Comparing Eq. (1) (or Eq. (22)), and Eq. (24), we get a difference of 38%.

In the case of the JLT model, with $K_j = 0.78$ the value of A is 5.037, then

$$M = \frac{2.5185 H_0^2 R_0^3}{G} = \frac{2.3404 R_0^3}{GT_0^2} = 5.8148 \times 10^{12} h^2 R_0^3 M_\odot \quad [25]$$

and then the difference with the case LT is 90%. Finally, in the case of the $J\eta$ LT model, $A = 6.05$

$$M = \frac{3.025 H_0^2 R_0^3}{G} = \frac{2.8111 R_0^3}{GT_0^2} = 6.9843 \times 10^{12} h^2 R_0^3 M_\odot \quad [26]$$

which means that the mass in this case is more than double of the case LT. The difference in mass between the previous cases is due to the modification of the perturbation evolution due to the effect of angular momentum, and dynamical friction as also shown in several papers Refs.(13–19).

The relation between mass, M , and turn-around radius, R_0 , may be obtained also from Eq. (17), Eq. (18), and Eq. (19), solving the equation $v(R_0) = 0$ with respect to M . In the case, LT, $A = 2.655$, and the $v - R$ relation is given by

$$v(R) = -1.038 \frac{GM}{R} + 1.196 H_0 R \quad [27]$$

and

$$M = 3.065 \times 10^{12} h^2 R_0^3 M_\odot \quad [28]$$

In Fig.4, we plot the $v - y(R)$ relations for the MLT, the JLT, and the $J\eta$ LT cases. For distances smaller than R_0 , the plot shows that the $J\eta$ LT cases gives larger negative velocities than the JLT model, and this larger negative velocities than the MLT model. This imply that the turn-around happens earlier in $J\eta$ LT with respect to the JLT model, and similarly the turn-around happens earlier in JLT with respect to the MLT model. One interesting point is that the mass obtained from the $M - R_0$ relation in the case SLT (Eq. (27)) is smaller than that of the MLT case (Eq. (17)). The last is smaller than the mass obtained with the JLT (Eq. (18)), and this is smaller than that of $J\eta$ LT case (Eq. (19)).

For example, fitting the data by means of Eq. (27) (case SLT), the mass is $\simeq 10\%$ smaller than that obtained with

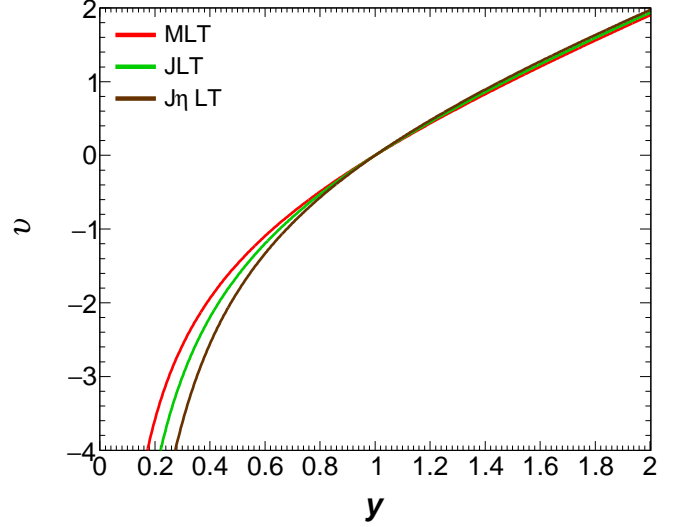


Fig. 4. $v - R$ relationship for the MLT model (red curve), JLT (green curve), and $J\eta$ LT (brown curve).

Eq. (17) (case MLT)[¶]. Fitting the data by means of Eq. (27), and Eq. (19) the mass differences become larger (10% in the case of M81, 100% in the case of NGC 253, and around 40% in the other cases, excluding Virgo).

The differences between the two methods can be explained as follows. In the method based on the fitting, the turn-around is obtained through $R_0 = (\frac{2GM}{AH_0^2})^{1/3}$, and depends from M , and H , obtained through the fit.

In the method based on the $M - R_0$ relation, R_0 is obtained by any method allowing the determination of this quantity, and then the $M - R_0$ relationship gives the mass.

Another interesting point, is the decrease of h from the SLT model, to the $J\eta$ LT model. The maximum differences for the groups and clusters studied is $\simeq 30\%$.

Stable structure	range of w
M81	$w \geq -1.5$
IC342	$w \geq -1$
NGC253	$w \geq -1$
GenA/M83	$w \geq -1.5$
Local Group	$w \geq -2$
Virgo	$w \geq -1.5$

Table 3. The allowed ranges of w .

Constraints on the DM EoS parameter

Recently, the turn-around radius, R_0 has been proposed as a promising way to test cosmological models Ref.(88), DE, and disentangle between Λ CDM model, DE, and MG models Refs.(88–93).

Ref.(89) calculated R_0 for Λ CDM, and Ref.(90) did the same for smooth DE. According to Ref.(93) R_0 is affected by modified gravity (MG) theories. In MG theories Ref.(94) found a general relation for R_0 , and Ref.(91) found a method

[¶]The differences between the SLT, and MLT given by the $M - R_0$ relations (Eqs.(22), (24)) is 38%.

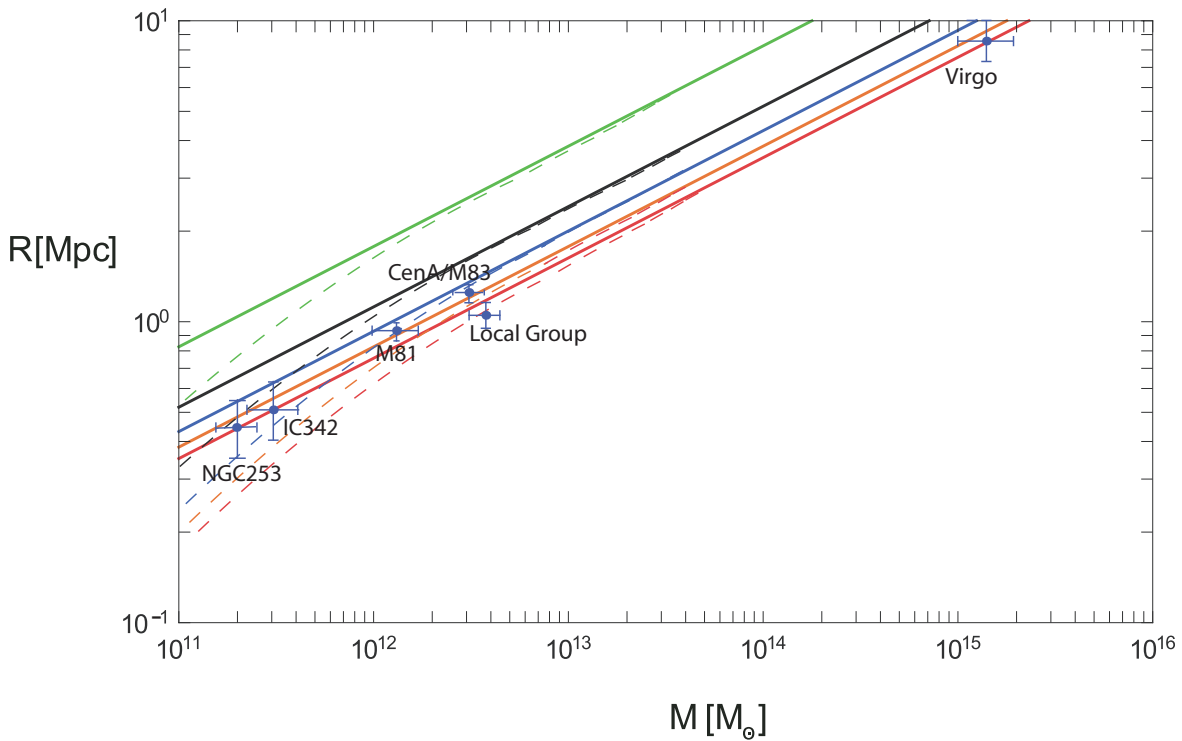


Fig. 5. Mass-radius relation of stable structures for different w . The solid lines from top to bottom represent $w = -0.5$ (solid green line), -1 (black solid line), -1.5 (blue solid line), -2 (pink solid line), -2.5 (red solid line). The dashed lines are the same of the previous lines, but they are obtained in Ref.(21). The dots with error bars taken from Table 2.

to get the same quantities in generic gravitational theories. In Ref.(21), we used an extended spherical collapse model (ESCM) introduced, and adopted in Refs.(66, 73, 95–97), to show how R_0 is modified by the presence of vorticity, and shear in the equation of motion. We also showed how the $M - R_0$ plane can be used to put some constraints on the DE EoS parameter w , similarly to Refs.(89, 90). The constraints on w depends on the estimated values of the mass and R_0 of galaxies, groups, and clusters. Some data were taken from Ref.(90), and others from Ref.(1, 2).

With the revised value of mass, M , and R_0 presented in this paper, we recalculate the constraints showed in Ref.(21).

Fig.5 plots the mass-radius relation of stable structures for different w . The solid lines from top to bottom represent $w = -0.5$ (solid green line), -1 (black solid line), -1.5 (blue solid line), -2 (pink solid line), -2.5 (red solid line). The dashed lines are the same of the previous lines, but they are obtained using the model from Ref.(21). The dots with error bars, are data obtained in the previous sections, and reported in Table 2 (case $J\eta$ LT).

The constraints to w are reproduced in Table 3. They are different from previous ones obtained by Ref.(89, 90) based on the calculation of the mass, M , and R_0 by means of the virial theorem or the LT model.

Conclusions

In this paper, we extended the modified LT (MLT) model Refs.(1, 2) to take account the effect of angular momentum and dynamical friction. The inclusion of these two quantities in the equation of motion modifies the evolution of perturbations as described by the MLT model. The collapse of shells

inside the zero-velocity surface collapse earlier when adding the angular momentum (JLT model), and dynamical friction term ($J\eta$ LT model). After solving the equation of motion, we got the relationships between mass, M , and the turn-around radius R_0 , similar to those obtained for the SLT model by Ref.(7), and for the MLT model by Refs.(1, 2). The relationships show, for a given R_0 , a larger mass of the perturbation when angular momentum, and dynamical friction are taken into account. If one can obtain by some method the value of the turn-around, these relations show that the perturbation mass is 90% (JLT model), and two times larger ($J\eta$ LT model) with respect to the SLT model. In the paper, we also found velocity, v , radius, R , relationships for the cases considered depending on mass and the Hubble constant. These were fitted to the data of the local group, M81, NGC 253, IC342, CenA/M83, and Virgo. The values of the masses obtained fitting the data by means of Eq. (19) ($J\eta$ LT model) are larger than those obtained by means of Eq. (27) (SLT model). The mass difference is 10% in the case of M81, 100% in the case of NGC 253, and around 40% in the other cases.

The Hubble parameter becomes smaller when introducing angular momentum, and dynamical friction with respect to the SLT model. The same happens when adding the cosmological constant to the SLT model, as noticed by Refs.(1, 2).

Finally, we used the mass, M , and R_0 for the studied objects to put constraints to w . The constraints obtained differ from those obtained in previous papers Refs.(89, 90) based on the calculation of the mass, M , and R_0 by means of the virial theorem or the LT model.

ACKNOWLEDGMENTS. The authors wish to express their grat-

itude to S. Peirani and A. De Freitas Pacheco for a fruitful discussion.

1. S. Peirani, J. A. de Freitas Pacheco, Mass determination of groups of galaxies: Effects of the cosmological constant, *New Astronomy* 11 (4) (2006) 325–330. [arXiv:astro-ph/0508614](#), [doi:10.1016/j.newast.2005.08.008](#).
2. S. Peirani, J. A. de Freitas Pacheco, Dynamics of nearby groups of galaxies: the role of the cosmological constant, *A&A* 488 (3) (2008) 845–851. [arXiv:0806.4245](#), [doi:10.1051/0004-6361:200809711](#).
3. J. P. Huchra, M. J. Geller, Groups of galaxies. I - Nearby groups, *ApJ* 257 (1982) 423–437. [doi:10.1086/160000](#).
4. I. Karachentsev, The Local Group and other neighboring galaxy groups, *Astron. J.* 129 (2005) 178. [arXiv:astro-ph/0410065](#), [doi:10.1086/426368](#).
5. S.-M. Niemi, P. Nurmi, P. Heinämäki, M. Valtonen, Are the nearby groups of galaxies gravitationally bound objects?, *MNRAS* 382 (4) (2007) 1864–1876. [arXiv:0709.3176](#), [doi:10.1111/j.1365-2966.2007.12498.x](#).
6. D. Lynden-Bell, The dynamical age of the local group of galaxies, *The Observatory* 101 (1981) 111–114.
7. A. Sandage, The Redshift-Distance Relation. IX. Perturbation of the Very Nearby Velocity Field by the Mass of the Local Group, *ApJ* 307 (1986) 1. [doi:10.1086/164387](#).
8. G. Lemaître, L'Univers en expansion, *Annales de la Societe Scientifique de Bruxelles* 53 (1933) 51.
9. R. C. Tolman, Effect of Inhomogeneity on Cosmological Models, *Proceedings of the National Academy of Science* 20 (3) (1934) 169–176. [doi:10.1073/pnas.20.3.169](#).
10. G. L. Hoffman, D. W. Olson, E. E. Salpeter, Dynamical models and the mass of the Virgo cluster, *ApJ* 242 (1980) 861–878. [doi:10.1086/158520](#).
11. R. B. Tully, E. J. Shaya, Infall of galaxies into the virgo cluster and some cosmological constraints, *ApJ* 281 (1984) 31–55. [doi:10.1086/162073](#).
12. P. Teerikorpi, L. Bottinelli, L. Gougenheim, G. Paturel, Investigations of the Local Supercluster velocity field. I. Observations close to Virgo, using Tully-Fisher distances and the Tolman-Bondi expanding sphere., *A&A* 260 (1992) 17–32.
13. A. Del Popolo, M. Gambera, Tidal torques and the clusters of galaxies evolution, *A&A* 337 (1998) 96–104. [arXiv:astro-ph/9802214](#).
14. A. Del Popolo, M. Gambera, The effect of non-radial motions on the X-ray temperature distribution function and the two-point correlation function of clusters, *A&A* 344 (1999) 17–26. [arXiv:astro-ph/9806044](#).
15. A. Del Popolo, M. Gambera, Non radial motions and the shapes and the abundance of clusters of galaxies, *A&A* 357 (2000) 809–815. [arXiv:astro-ph/9909156](#).
16. A. Del Popolo, The excursion set approach, and an improved model for the multiplicity function, *A&A* 448 (2006) 439–446. [doi:10.1051/0004-6361:20053526](#).
17. A. Del Popolo, Evolution of the Cosmological Mass Function in a Moving Barrier Model, *AJ* 131 (2006) 2367–2372. [arXiv:astro-ph/0609101](#), [doi:10.1086/503163](#).
18. A. Del Popolo, Some improvements to the spherical collapse model, *A&A* 454 (2006) 17–26. [arXiv:0801.1086](#), [doi:10.1051/0004-6361:20054441](#).
19. A. Del Popolo, F. Pace, M. Le Delliou, A high precision semi-analytic mass function, *JCAP* 3 (2017) 032. [arXiv:1703.06918](#), [doi:10.1088/1475-7516/2017/03/032](#).
20. A. Del Popolo, F. Pace, D. F. Mota, Mass-temperature relation in Λ CDM and modified gravity, *PRD* 100 (2) (2019) 024013. [arXiv:1908.07322](#), [doi:10.1103/PhysRevD.100.024013](#).
21. A. Del Popolo, M. H. Chan, D. F. Mota, Turnaround radius in Λ CDM and dark matter cosmologies with shear and vorticity, *PRD* 101 (8) (2020) 083505. [doi:10.1103/PhysRevD.101.083505](#).
22. J. E. Gunn, J. R. Gott, III, On the Infall of Matter Into Clusters of Galaxies and Some Effects on Their Evolution, *ApJ* 176 (1972) 1. [doi:10.1086/151605](#).
23. J. Silk, Large-Scale Inhomogeneity of the Universe: Implications for the Deceleration Parameter, *ApJ* 193 (1974) 525–528. [doi:10.1086/153189](#).
24. J. E. Gunn, Massive galactic halos. I - Formation and evolution, *ApJ* 218 (1977) 592–598. [doi:10.1086/155715](#).
25. P. J. E. Peebles, Origin of the Angular Momentum of Galaxies, *ApJ* 155 (1969) 393. [doi:10.1086/149876](#).
26. S. D. M. White, Angular momentum growth in protogalaxies, *ApJ* 286 (1984) 38–41. [doi:10.1086/162573](#).
27. B. S. Ryden, J. E. Gunn, Galaxy formation by gravitational collapse, *ApJ* 318 (1987) 15–31. [doi:10.1086/165349](#).
28. B. S. Ryden, Galaxy formation - The role of tidal torques and dissipational infall, *ApJ* 329 (1988) 589–611. [doi:10.1086/166406](#).
29. L. L. R. Williams, A. Babul, J. P. Dalcanton, Investigating the Origins of Dark Matter Halo Density Profiles, *ApJ* 604 (2004) 18–39. [arXiv:astro-ph/0312002](#), [doi:10.1086/381722](#).
30. V. Antonuccio-Delogu, S. Colafrancesco, Dynamical friction, secondary infall, and the evolution of clusters of galaxies, *ApJ* 427 (1994) 72–85. [doi:10.1086/174122](#).
31. A. Del Popolo, The Cusp/Core Problem and the Secondary Infall Model, *ApJ* 698 (2009) 2093–2113. [arXiv:0906.4447](#), [doi:10.1088/0004-637X/698/2/2093](#).
32. J. A. Fillmore, P. Goldreich, Self-similar gravitational collapse in an expanding universe, *ApJ* 281 (1984) 1–8. [doi:10.1086/162070](#).
33. E. Bertschinger, Self-similar secondary infall and accretion in an Einstein-de Sitter universe, *ApJ* 558 (1985) 39–65. [doi:10.1086/191028](#).
34. Y. Hoffman, J. Shaham, Local density maxima - Progenitors of structure, *ApJ* 297 (1985) 16–22. [doi:10.1086/163498](#).
35. K. Subramanian, R. Cen, J. P. Ostriker, The Structure of Dark Matter Halos in Hierarchical Clustering Theories, *ApJ* 538 (2000) 528–542. [arXiv:astro-ph/9909279](#), [doi:10.1086/309152](#).
36. Y. Ascasibar, G. Yepes, S. Gottlöber, V. Müller, On the physical origin of dark matter density profiles, *MNRAS* 352 (2004) 1109–1120. [arXiv:astro-ph/0312221](#), [doi:10.1111/j.1365-2966.2004.08005.x](#).
37. O. Lahav, P. B. Lilje, J. R. Primack, M. J. Rees, Dynamical effects of the cosmological constant, *MNRAS* 251 (1991) 128–136.
38. A. V. Gurevich, K. P. Zybin, Nondissipative gravitational turbulence, *Zhurnal Eksperimentalnoi i Teoreticheskoi Fiziki* 94 (1988) 3–25.
39. A. V. Gurevich, K. P. Zybin, Nondissipative gravitational turbulence in the expanding Universe, *Zhurnal Eksperimentalnoi i Teoreticheskoi Fiziki* 94 (1988) 5–15.
40. S. D. M. White, D. Zaritsky, Models for Galaxy halos in an open universe, *ApJ* 394 (1992) 1–6. [doi:10.1086/171552](#).
41. P. Sikivie, I. I. Tkachev, Y. Wang, Secondary infall model of galactic halo formation and the spectrum of cold dark matter particles on Earth, *PRD* 56 (1997) 1863–1878. [arXiv:astro-ph/9609022](#), [doi:10.1103/PhysRevD.56.1863](#).
42. A. Nusser, Self-similar spherical collapse with non-radial motions, *MNRAS* 325 (2001) 1397–1401. [arXiv:astro-ph/0008217](#), [doi:10.1046/j.1365-8711.2001.04527.x](#).
43. N. Hiotelis, Density profiles in a spherical infall model with non-radial motions, *A&A* 382 (2002) 84–91. [arXiv:astro-ph/0111324](#), [doi:10.1051/0004-6361:20011620](#).
44. M. Le Delliou, R. N. Henriksen, Non-radial motion and the NFW profile, *A&A* 408 (2003) 27–38. [arXiv:astro-ph/0307046](#), [doi:10.1051/0004-6361:20030922](#).
45. P. Zukin, E. Bertschinger, A Generalized Secondary Infall Model, in: *APS Meeting Abstracts*, 2010, p. 13003.
46. Y. Hoffman, The dynamics of superclusters - The effect of shear, *ApJ* 308 (1986) 493–498. [doi:10.1086/164520](#).
47. Y. Hoffman, Dynamics of superclusters - Reconciling $\Omega(0) = 1.0$ with observations?, *ApJ* 340 (1989) 69–76. [doi:10.1086/167376](#).
48. S. Zaroubi, Y. Hoffman, Gravitational Collapse in an Expanding Universe: Asymptotic Self-similar Solutions, *ApJ* 416 (1993) 410. [doi:10.1086/173246](#).
49. F. Bernardreau, Skewness and kurtosis in large-scale cosmic fields, *ApJ* 433 (1994) 1–18. [arXiv:astro-ph/9312026](#), [doi:10.1086/174620](#).
50. J. M. Bardeen, J. R. Bond, N. Kaiser, A. S. Szalay, The statistics of peaks of Gaussian random fields, *ApJ* 304 (1986) 15–61. [doi:10.1086/164143](#).
51. Y. Ohta, I. Kayo, A. Taruya, Evolution of the Cosmological Density Distribution Function from the Local Collapse Model, *ApJ* 589 (2003) 1–16. [arXiv:astro-ph/0301567](#), [doi:10.1086/374375](#).
52. Y. Ohta, I. Kayo, A. Taruya, Cosmological Density Distribution Function from the Ellipsoidal Collapse Model in Real Space, *ApJ* 608 (2004) 647–662. [arXiv:astro-ph/0402618](#), [doi:10.1086/420762](#).
53. S. Basilakos, Cosmological implications and structure formation from a time varying vacuum, *MNRAS* 395 (2009) 2347–2355. [arXiv:0903.0452](#), [doi:10.1111/j.1365-2966.2009.14713.x](#).
54. F. Pace, J.-C. Waizmann, M. Bartelmann, Spherical collapse model in dark-energy cosmologies, *MNRAS* 406 (2010) 1865–1874. [arXiv:1005.0233](#), [doi:10.1111/j.1365-2966.2010.16841.x](#).
55. S. Basilakos, M. Plionis, J. Solà, Spherical collapse model in time varying vacuum cosmologies, *PRD* 82 (8) (2010) 083512. [arXiv:1005.5592](#), [doi:10.1103/PhysRevD.82.083512](#).
56. D. F. Mota, C. van de Bruck, On the spherical collapse model in dark energy cosmologies, *A&A* 421 (2004) 71–81. [arXiv:astro-ph/0401504](#), [doi:10.1051/0004-6361:20041090](#).
57. N. J. Nunes, D. F. Mota, Structure formation in inhomogeneous dark energy models, *MNRAS* 368 (2006) 751–758. [arXiv:astro-ph/0409481](#), [doi:10.1111/j.1365-2966.2006.10166.x](#).
58. L. R. Abramo, R. C. Batista, L. Liberato, R. Rosenfeld, Structure formation in the presence of dark energy perturbations, *Journal of Cosmology and Astro-Particle Physics* 11 (2007) 12–+. [arXiv:0707.2882](#), [doi:10.1088/1475-7516/2007/11/012](#).
59. L. R. Abramo, R. C. Batista, L. Liberato, R. Rosenfeld, Dynamical mutation of dark energy, *PRD* 77 (6) (2008) 067301–+. [arXiv:0710.2368](#), [doi:10.1103/PhysRevD.77.067301](#).
60. L. R. Abramo, R. C. Batista, R. Rosenfeld, The signature of dark energy perturbations in galaxy cluster surveys, *Journal of Cosmology and Astro-Particle Physics* 7 (2009) 40–+. [arXiv:0902.3226](#), [doi:10.1088/1475-7516/2009/07/040](#).
61. L. R. Abramo, R. C. Batista, L. Liberato, R. Rosenfeld, Physical approximations for the non-linear evolution of perturbations in inhomogeneous dark energy scenarios, *PRD* 79 (2) (2009) 023516–+. [arXiv:0806.3461](#), [doi:10.1103/PhysRevD.79.023516](#).
62. P. Creminelli, G. D'Amico, J. Noreña, L. Senatore, F. Vernizzi, Spherical collapse in quintessence models with zero speed of sound, *JCAP* 3 (2010) 27. [arXiv:0911.2701](#), [doi:10.1088/1475-7516/2010/03/027](#).
63. T. Basse, O. Eggers Bjælde, Y. Y. Y. Wong, Spherical collapse of dark energy with an arbitrary sound speed, *JCAP* 10 (2011) 38. [arXiv:1009.0010](#), [doi:10.1088/1475-7516/2011/10/038](#).
64. R. C. Batista, F. Pace, Structure formation in inhomogeneous Early Dark Energy models, *JCAP* 6 (2013) 44. [arXiv:1303.0414](#), [doi:10.1088/1475-7516/2013/06/044](#).
65. A. Del Popolo, F. Pace, J. A. S. Lima, Spherical collapse model with shear and angular momentum in dark energy cosmologies, *MNRAS* 430 (2013) 628–637. [arXiv:1212.5092](#), [doi:10.1093/mnras/sts669](#).
66. A. Del Popolo, F. Pace, J. A. S. Lima, Extended Spherical Collapse and the Accelerating Universe, *International Journal of Modern Physics D* 22 (2013) 50038. [arXiv:1207.5789](#), [doi:10.1142/S0218271813500387](#).
67. F. Pace, R. C. Batista, A. Del Popolo, Effects of shear and rotation on the spherical collapse model for clustering dark energy, *MNRAS* 445 (2014) 648–659. [arXiv:1406.1448](#), [doi:10.1093/mnras/stu1782](#).
68. A. Del Popolo, F. Pace, S. P. Maydanyuk, J. A. S. Lima, J. F. Jesus, Shear and rotation in Chaplygin cosmology, *PRD* 87 (4) (2013) 043527. [arXiv:1303.3628](#), [doi:10.1103/PhysRevD.87.043527](#).
69. P. J. E. Peebles, *Principles of physical cosmology*, 1993.
70. J. G. Bartlett, J. Silk, Galaxy clusters and the COBE result, *ApJ* 407 (1993) L45–L48. [doi:10.1086/186802](#).
71. P. Fosalba, E. Gaztañaga, *Cosmological Perturbation Theory and the Spheri-*

- cal Collapse model - I. Gaussian initial conditions, *MNRAS*301 (1998) 503–523. [arXiv:astro-ph/9712095](#), [doi:10.1046/j.1365-8711.1998.02033.x](#).
72. S. Engineer, N. Kanekar, T. Padmanabhan, Non-linear density evolution from an improved spherical collapse model, *MNRAS*314 (2000) 279–289. [arXiv:astro-ph/9812452](#), [doi:10.1046/j.1365-8711.2000.03275.x](#).
 73. F. Pace, C. Schmid, D. F. Mota, A. D. Popolo, Halo collapse: virialization by shear and rotation in dynamical dark-energy models. effects on weak-lensing peaks, *Journal of Cosmology and Astroparticle Physics* 2019 (09) (2019) 060–060. [doi:10.1088/1475-7516/2019/09/060](#).
<https://doi.org/10.1088/2F1475-7516%2F2019%2F09%2F060>
 74. J. S. Bullock, T. S. Kolatt, Y. Sigad, R. S. Somerville, A. V. Kravtsov, A. A. Klypin, J. R. Primack, A. Dekel, Profiles of dark haloes: evolution, scatter and environment, *MNRAS*321 (2001) 559–575. [arXiv:astro-ph/9908159](#), [doi:10.1046/j.1365-8711.2001.04068.x](#).
 75. I. D. Karachentsev, M. E. Sharina, D. I. Makarov, A. E. Dolphin, E. K. Grebel, D. Geisler, P. Guhathakurta, P. W. Hodge, V. E. Karachentseva, A. Sarajedini, P. Seitzer, The very local Hubble flow, *A&A*389 (2002) 812–824. [arXiv:astro-ph/0204507](#), [doi:10.1051/0004-6361:20020649](#).
 76. I. D. Karachentsev, A. E. Dolphin, D. Geisler, E. K. Grebel, P. Guhathakurta, P. W. Hodge, V. E. Karachentseva, A. Sarajedini, P. Seitzer, M. E. Sharina, The M 81 group of galaxies: New distances, kinematics and structure, *A&A*383 (2002) 125–136. [doi:10.1051/0004-6361:20011741](#).
 77. I. D. Karachentsev, A. Dolphin, R. B. Tully, M. Sharina, L. Makarova, D. Makarov, V. Karachentseva, S. Sakai, E. J. Shaya, Advanced Camera for Surveys Imaging of 25 Galaxies in Nearby Groups and in the Field, *AJ*131 (3) (2006) 1361–1376. [arXiv:astro-ph/0511648](#), [doi:10.1086/500013](#).
 78. I. D. Karachentsev, E. K. Grebel, M. E. Sharina, A. E. Dolphin, D. Geisler, P. Guhathakurta, P. W. Hodge, V. E. Karachentseva, A. Sarajedini, P. Seitzer, Distances to nearby galaxies in Sculptor, *A&A*404 (2003) 93–111. [arXiv:astro-ph/0302045](#), [doi:10.1051/0004-6361:20030170](#).
 79. I. D. Karachentsev, M. E. Sharina, A. E. Dolphin, E. K. Grebel, Distances to nearby galaxies around IC 342, *A&A*408 (2003) 111–118. [doi:10.1051/0004-6361:20030912](#).
 80. I. D. Karachentsev, M. E. Sharina, A. E. Dolphin, E. K. Grebel, D. Geisler, P. Guhathakurta, P. W. Hodge, V. E. Karachentseva, A. Sarajedini, P. Seitzer, New distances to galaxies in the Centaurus A group, *A&A*385 (2002) 21–31. [doi:10.1051/0004-6361:20020042](#).
 81. I. D. Karachentsev, R. B. Tully, A. Dolphin, M. Sharina, L. Makarova, D. Makarov, S. Sakai, E. J. Shaya, O. G. Kashibadze, V. Karachentseva, L. Rizzi, The Hubble Flow around the Centaurus A/M83 Galaxy Complex, *AJ*133 (2) (2007) 504–517. [arXiv:astro-ph/0603091](#), [doi:10.1086/510125](#).
 82. K. A. Woodley, The Centaurus Group and the Outer Halo of NGC 5128: Are They Dynamically Connected?, *AJ*132 (6) (2006) 2424–2431. [arXiv:astro-ph/0608497](#), [doi:10.1086/508631](#).
 83. P. Fouque, J. M. Solanes, T. Sanchis, C. Balkowski, Structure, mass and distance of the virgo cluster from a tolmán-bondi model, *Astronomy and Astrophysics* 375 (3) (2001) 770–780. [doi:10.1051/0004-6361:20010833](#).
<http://dx.doi.org/10.1051/0004-6361:20010833>
 84. W. L. Freedman, B. F. Madore, D. Hatt, T. J. Hoyt, I. S. Jang, R. L. Beaton, C. R. Burns, M. G. Lee, A. J. Monson, J. R. Neeley, M. M. Phillips, J. A. Rich, M. Seibert, The Carnegie-Chicago Hubble Program. VIII. An Independent Determination of the Hubble Constant Based on the Tip of the Red Giant Branch, *ApJ*882 (1) (2019) 34. [arXiv:1907.05922](#), [doi:10.3847/1538-4357/ab2f73](#).
 85. K. Hotokezaka, E. Nakar, O. Gottlieb, S. Nissanke, K. Masuda, G. Hallinan, K. P. Mooley, A. T. Deller, A Hubble constant measurement from superluminal motion of the jet in GW170817, *Nature Astronomy* 3 (2019) 940–944. [arXiv:1806.10596](#), [doi:10.1038/s41550-019-0820-1](#).
 86. N. Schöneberg, J. Lesgourgues, D. C. Hooper, The BAO+BBN take on the Hubble tension, *JCAP*2019 (10) (2019) 029. [arXiv:1907.11594](#), [doi:10.1088/1475-7516/2019/10/029](#).
 87. O. Müller, H. Jerjen, B. Binggeli, New low surface brightness dwarf galaxies in the Centaurus group, *A&A*597 (2017) A7. [arXiv:1605.04130](#), [doi:10.1051/0004-6361/201628921](#).
 88. R. C. C. Lopes, R. Voivodic, L. R. Abramo, J. Sodré, Laerte, Turnaround radius in f(R) model, *JCAP*2018 (9) (2018) 010. [arXiv:1805.09918](#), [doi:10.1088/1475-7516/2018/09/010](#).
 89. V. Pavlidou, T. N. Tomaras, Where the world stands still: turnaround as a strong test of Λ CDM cosmology, *JCAP*2014 (9) (2014) 020. [arXiv:1310.1920](#), [doi:10.1088/1475-7516/2014/09/020](#).
 90. V. Pavlidou, N. Tetradis, T. N. Tomaras, Constraining dark energy through the stability of cosmic structures, *JCAP*2014 (5) (2014) 017. [arXiv:1401.3742](#), [doi:10.1088/1475-7516/2014/05/017](#).
 91. V. Faraoni, M. Lapiere-Léonard, A. Prain, Turnaround radius in an accelerated universe with quasi-local mass, *JCAP*2015 (10) (2015) 013. [arXiv:1508.01725](#), [doi:10.1088/1475-7516/2015/10/013](#).
 92. S. Bhattacharya, K. F. Dialektopoulos, A. Enea Romano, C. Skordis, T. N. Tomaras, The maximum sizes of large scale structures in alternative theories of gravity, *JCAP*7 (2017) 018. [arXiv:1611.05055](#), [doi:10.1088/1475-7516/2017/07/018](#).
 93. R. C. C. Lopes, R. Voivodic, L. R. Abramo, J. Sodré, Laerte, Relation between the turnaround radius and virial mass in f(R) model, *JCAP*2019 (7) (2019) 026. [arXiv:1809.10321](#), [doi:10.1088/1475-7516/2019/07/026](#).
 94. S. Capozziello, K. F. Dialektopoulos, O. Luongo, Maximum turnaround radius in f(R) gravity, *International Journal of Modern Physics D* 28 (3) (2019) 1950058. [arXiv:1805.01233](#), [doi:10.1142/S0218271819500585](#).
 95. A. Del Popolo, Non-baryonic dark matter in cosmology, in: *AIP Conf. Proc.*, Vol. 1548, 2013, pp. 2–63. [doi:10.1063/1.4817029](#).
 96. F. Pace, R. C. Batista, A. Del Popolo, Effects of shear and rotation on the spherical collapse model for clustering dark energy, *MNRAS*445 (1) (2014) 648–659. [arXiv:1406.1448](#), [doi:10.1093/mnras/stu1782](#).
 97. A. Mehrabi, F. Pace, M. Malekjani, A. Del Popolo, Constraints on shear and rotation with massive galaxy clusters, *MNRAS*465 (3) (2017) 2687–2697. [arXiv:1608.07961](#), [doi:10.1093/mnras/stw2927](#).